

Acid-Stable Magnetic Core–Shell Nanoparticles for the Separation of Rare Earths

David Dupont,[†] Jakob Luyten,[†] Maarten Bloemen,[‡] Thierry Verbiest,[‡] and Koen Binnemans^{*†}

[†]Molecular Design and Synthesis, Department of Chemistry, and [‡]Molecular Imaging and Photonics, Department of Chemistry, KU Leuven, B-3001 Heverlee, Belgium

S Supporting Information

ABSTRACT: Core–shell $\text{Fe}_3\text{O}_4@/\text{SiO}_2$ nanoparticles were prepared with a modified Stöber method and functionalized with *N*-[(3-trimethoxysilyl)propyl]ethylenediamine triacetic acid (TMS-EDTA). The synthesis was optimized to make core–shell nanoparticles with homogeneous and thin SiO_2 shells (4.8 ± 0.5 nm) around highly superparamagnetic Fe_3O_4 cores (14.5 ± 3.0 nm). The core–shell $\text{Fe}_3\text{O}_4@/\text{SiO}_2$ (TMS-EDTA) nanoparticles were then used for the extraction and separation of rare-earth ions. By comparing them with previously published results for Fe_3O_4 (TMS-EDTA) and SiO_2 (TMS-EDTA) nanoparticles, it was clear that the core–shell nanoparticles combine the advantage of magnetic retrieval observed for Fe_3O_4 (TMS-EDTA) nanoparticles with the higher selectivity observed for SiO_2 (TMS-EDTA). The advantages of the SiO_2 shell include a lower specific weight and a larger grafting density compared to Fe_3O_4 surfaces, but also the improved resistance to acidic environments required for the stripping of rare-earth ions.

1. INTRODUCTION

Magnetic nanoparticles are very interesting materials that can be recovered from solution with the use of a magnet.^{1–3} Task-specific magnetic nanoparticles can be prepared by coating the surface with functional groups.^{2,3} Applications are found in targeted drug delivery, biosensors, dual imaging compounds, recoverable catalysts, and selective recovery of metal ions or molecules.^{3–15} Functionalized magnetic nanoparticles are well-suited for the selective extraction of metal traces from diluted wastewater streams or industrial effluents.^{7–20} This is done by capturing metal ions in solution, retrieving the loaded nanoparticles with a magnet, and then stripping the metal ions from the nanoparticles. This is a sustainable process since the nanoparticles are reusable and no hazardous chemicals are involved. Most examples report on the recovery of transition metals, heavy metals, or precious metals.^{7–25} On the other hand, the capture of rare-earth ions has been far less investigated.^{16,21,26}

Core–shell nanoparticles are slightly more complex than conventional nanoparticles, but these hybrid materials can have significantly enhanced properties.^{27–29} The core is usually a magnetic and vulnerable material such as magnetite or cobalt that is prone to oxidation or dissolution in acidic environments. These cores are capped with an inert shell of, e.g., SiO_2 , TiO_2 , ZrO_2 , gold, graphene, or a polymer.^{3,30–32} The shell protects the core from oxidation or attack by chemicals, and it can be further functionalized by attaching functional groups to its surface.^{3,16,21–24} The advantage of layered materials can be the better stability or a synergy between different materials, which can result in unique chemical or physical properties.^{27–29}

Functionalization of core–shell and regular nanoparticles can be achieved by covalent bonding, chemisorption, or electrostatic interactions of ligands onto their surface. Good results have been obtained with functionalized siloxanes, because these versatile compounds form strong covalent bonds with most

oxide surfaces due to the presence of hydroxyl groups.^{33–37} The large number of commercially available trialkoxysilanes with various functional groups offers unique possibilities for the task-specific surface modification of oxide nanoparticles.^{16,35,38–41} The *N*-[(3-trimethoxysilyl)propyl]ethylenediamine triacetic acid (TMS-EDTA) used in this work is an EDTA derivative in which one of the carboxylate groups is replaced by an alkyl spacer with a reactive trialkoxysilane group for binding to the surface of the nanoparticle. EDTA has a good affinity for rare-earth ions and is also capable of separating them based on small differences in charge density.^{42–44} TMS-EDTA was therefore the preferred ligand to decorate the surface of the nanoparticles. The covalently bonded TMS-EDTA also provides nanoparticles with a good resistance against the strongly acidic environments required for the stripping of rare-earth ions after coordination (pH < 2).²⁶

Recently, our group compared the adsorption capacity and selectivity of TMS-EDTA-functionalized Fe_3O_4 , TiO_2 , and SiO_2 nanoparticles to gain a better understanding of the influence of the substrate on the behavior of the surface group.²⁶ It was shown that TMS-EDTA-functionalized SiO_2 nanoparticles performed better than the analogous Fe_3O_4 or TiO_2 nanoparticles. This was attributed to the fact that SiO_2 contains the highest density of hydroxyl groups on its surface, resulting in a large grafting density of TMS-EDTA functional groups. This dense layer of TMS-EDTA groups is capable of binding high quantities of rare-earth ions, but it also exhibits a significant size-based selectivity. It was shown that a denser layer of TMS-EDTA results in a better separation between small and large rare-earth ions. However, both SiO_2 and TiO_2 nanoparticles are

Received: June 24, 2014

Revised: August 31, 2014

Accepted: September 3, 2014

Published: September 3, 2014

not magnetic, so their removal from solution is much more tedious than the fast magnetic retrieval that is possible for Fe_3O_4 nanoparticles. In this paper, core-shell nanoparticles were prepared consisting of magnetic Fe_3O_4 cores and a SiO_2 shell, which was subsequently functionalized with TMS-EDTA (Figure 1). The aim was to investigate whether these

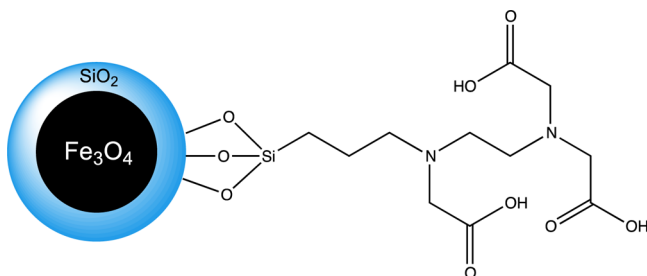


Figure 1. Core-shell $\text{Fe}_3\text{O}_4@/\text{SiO}_2$ nanoparticle functionalized with TMS-EDTA.

functionalized core-shell nanoparticles could combine the advantage of magnetic retrieval, with the enhanced selectivity that was observed for TMS-EDTA attached to SiO_2 nanoparticles. The chemical stability and loss of efficiency of these core-shell nanoparticles were also investigated to evaluate their potential as high-performance, reusable sorbents for rare-earth ions.

2. EXPERIMENTAL SECTION

Chemicals. *N*-[(3-Trimethoxysilyl)propyl]ethylenediamine triacetic acid trisodium salt (TMS-EDTA) (45 wt %) was obtained from ABCR chemicals. Anhydrous FeCl_3 (97%) was purchased from Sigma-Aldrich. Ammonia (25 wt %) was obtained from Chem-Lab. Methanol (HPLC grade), absolute ethanol, glacial acetic acid, NaOH (97%), and HCl (37%) were purchased from VWR. $\text{Sm}(\text{NO}_3)_3 \cdot 6\text{H}_2\text{O}$ (99.9%), $\text{Gd}(\text{NO}_3)_3 \cdot 6\text{H}_2\text{O}$ (99.9%), $\text{Er}(\text{NO}_3)_3 \cdot 5\text{H}_2\text{O}$ (99.9%), *n*-octylamine (NOA) (99.9%), and tetraethyl orthosilicate (TEOS) (98%) were purchased from Acros Organics. $\text{La}(\text{NO}_3)_3 \cdot 6\text{H}_2\text{O}$ (99.9%) and $\text{Pr}(\text{NO}_3)_3 \cdot 6\text{H}_2\text{O}$ (99.9%) were supplied by Chempur. $\text{Nd}(\text{NO}_3)_3 \cdot 6\text{H}_2\text{O}$ (99.9%), $\text{Tb}(\text{NO}_3)_3 \cdot 5\text{H}_2\text{O}$ (99.9%), $\text{Dy}(\text{NO}_3)_3 \cdot 5\text{H}_2\text{O}$ (99.9%), and $\text{Ho}(\text{NO}_3)_3 \cdot 5\text{H}_2\text{O}$ (99.9%) were supplied by Alfa Aesar. All chemicals were used as received without further purification.

Equipment and Characterization. The nanoparticles were dispersed in a solvent using a Branson 5510 (10 L) and a Branson 2510 MTH (3 L) ultrasonic bath. The shaking during adsorption experiments was done with a mechanical shaker (IKA KS 130 basic). Particle imaging was done on a JEOL JEM2100 transmission electron microscope (TEM) using an acceleration voltage of 80 or 200 kV. ImageJ software was used for the size determination. The particles were dispersed in methanol (1 mg/mL) and deposited on a grid by solvent evaporation. Specific surface measurements were done by collecting nitrogen physisorption isotherms using a Micromeritics 3Flex surface characterization analyzer at 77 K. Prior to the measurement, the samples were outgassed at 353 K for 6 h under vacuum (Micromeritics VacPrep system). The BET method was applied in the 0.05–0.3 p/p_0 range using the 3Flex 3.00 software. Magnetization data were obtained with vibrating sample magnetometry (VSM) experiments performed on a VSM Maglab setup from Oxford Instruments at 300 K. Fourier transform infrared (FTIR) spectra were measured

between 4000 and 400 cm^{-1} on a Bruker Vertex 70 spectrometer, with a platinum ATR module. Thermogravimetric analysis (TGA) was performed with a TA Instruments Q600 thermogravimeter, measuring from 25 to $1200\text{ }^\circ\text{C}$ ($10\text{ }^\circ\text{C}/\text{min}$, argon atmosphere). A CE Instruments EA-1110 elemental analyzer was used to measure the carbon, hydrogen, and nitrogen (CHN) content of the functionalized nanoparticles. The rare-earth concentrations were determined by total reflection X-ray fluorescence (TXRF) analysis on a benchtop Bruker S2 Picofox TXRF spectrometer equipped with a molybdenum X-ray source. This technique allows direct determination of the rare-earth content on the nanoparticles in dispersion. This is a major advantage of TXRF compared to inductively coupled plasma mass spectrometric (ICP-MS) analysis, where nanoparticles have to be digested in acid prior to analysis. For the sample preparation, Eppendorf microtubes were filled with an amount of sample solution ($900\text{ }\mu\text{L}$) and a similar concentration (10–100 ppm) of Ga^{3+} as internal standard (1000 ppm gallium dissolved in 2–3% HNO_3 , Merck). Gallium was chosen because this element has a high sensitivity and does not interfere with the lanthanide signals. The microtubes were then vigorously shaken on a vibrating plate (IKA MS 3 basic). Finally, a $7\text{ }\mu\text{L}$ drop of this solution was put on a quartz plate, previously treated with a silicone/isopropyl alcohol solution (Serva) to avoid spreading of the sample droplet. The plates were then dried for 30 min at $60\text{ }^\circ\text{C}$ prior to analysis. Each sample was measured for 30 min.

Synthesis of $\text{Fe}_3\text{O}_4@/\text{SiO}_2$ Nanoparticles. An in-house synthesis procedure was followed to prepare precursor Fe_3O_4 nanoparticles coated with *n*-octylamine.⁴⁵ Ethylene glycol (37.5 mL) and *n*-octylamine (NOA; 25 mL) were combined into a flask and heated to $150\text{ }^\circ\text{C}$. Anhydrous FeCl_3 (2.4 g) was dissolved in a beaker containing ethylene glycol (10 mL) and Milli-Q water (3.0 mL). The iron(III) solution was slowly added to the flask containing ethylene glycol and *n*-octylamine, and further heated to reflux at $180\text{ }^\circ\text{C}$ for 24 h. The particles were precipitated from the reaction mixture by a small magnet and washed three times with acetone. Finally, they were dried in vacuo at room temperature for 20 min to obtain a black powder of Fe_3O_4 (NOA) nanoparticles with a typical yield of 1 g. The silica shell was grown on these seeds using a modified and optimized Stöber method.^{22,31} Fe_3O_4 (NOA) nanoparticles (50 mg) were dispersed in ethanol (40 mL) by placing them in an ultrasonic bath for 1 h. Without removing the solution from the sonicator bath, NH_3 (25%; 2 mL) was added to the nanoparticle dispersion and TEOS (0.8 mL) was added dropwise over an hour. The solution was then left in the sonicator bath for another 5 h. The nanoparticles were settled using centrifugation (11 000 rpm, 15 min) and washed one time with water and two times with acetone. Finally, they were dried in vacuo (room temperature (RT)) for 30 min to obtain a grayish powder with a typical yield of 100 mg.

Functionalization Protocol. The $\text{Fe}_3\text{O}_4@/\text{SiO}_2$ nanoparticles were functionalized with TMS-EDTA. The silanization procedure started by setting the pH at 4.5 with HCl (1 M) and then dispersing 100 mg of nanoparticles in MeOH/ H_2O 85:15 (100 mL). The beaker was placed in an ultrasonic bath for 2 h. TMS-EDTA (1 mmol) was then added together with a few drops of glacial acetic acid. The beaker was placed for another 2 h in the ultrasonic bath. The particles were precipitated from the reaction mixture by a small magnet and washed one time with water and two times with acetone. Finally, they were dried

in vacuo at room temperature for 30 min, resulting in $\text{Fe}_3\text{O}_4@\text{SiO}_2(\text{TMS-EDTA})$ with a typical yield of 95–100 mg.

Procedure for Adsorption and Stripping Experiments.

The TMS-EDTA functionalized core–shell nanoparticles were used to adsorb rare-earth ions from nitrate solutions and to separate rare-earth pairs. Adsorption and separation experiments started by dispersing 5 mg of nanoparticles in 5 mL of Milli-Q water using an ultrasonic bath (1 h). After a homogeneous dispersion of nanoparticles was obtained, single and binary rare-earth nitrate solutions were used to obtain the desired concentration of rare earths (1 mmol/L). This corresponds to 1 μmol of rare-earth ions per milligram of nanoparticles (an excess compared to the EDTA content). The pH was set using HCl (0.1 M) or NaOH (0.1 M), and the vials were placed on a mechanical shaker (240 rpm, 18 h). The particles were settled using a small NdFeB magnet. The solution was removed and the nanoparticles were washed two times with acetone to remove the remaining aqueous feed solution without influencing the adsorption equilibrium. The nanoparticles were then redispersed in 1 mL of Milli-Q water and the rare-earth content on the nanoparticles was analyzed with TXRF. The stripping of rare-earth ions from the nanoparticles was done by redispersing the washed nanoparticles in water (5 mL) and lowering the pH to 1.5 using an acidic HCl solution (1 M). The solution was then shaken for 2 h on a mechanical shaker (240 rpm).

3. RESULTS AND DISCUSSION

Optimizing the Synthesis of $\text{Fe}_3\text{O}_4@\text{SiO}_2(\text{TMS-EDTA})$ Nanoparticles. The magnetite nanoparticles were synthesized using a forced hydrolysis method.^{26,45} The Fe_3O_4 nanoparticles are capped with *n*-octylamine to protect their surface and can be stored for months.⁴⁵ However, this weakly bound coating can be replaced by siloxane molecules in a later stage to allow further modification of the nanoparticle surface with functional groups or SiO_2 shells.^{26,45} The synthesis of the SiO_2 shell and the functionalization with TMS-EDTA was investigated in detail and optimized for its use as nanosorbent. A modified Stöber method was used to grow SiO_2 shells around the Fe_3O_4 seeds with an average yield of 100 mg per batch. The thickness of the SiO_2 shell around the magnetite core could be tuned by varying the NH_3/TEOS ratio but was also influenced by other parameters such as the solvent/reagent ratio.³² The thickness is related to the size of the Si–O–Si band in the infrared spectrum at 1091 cm^{-1} (Figure 2). Methods A and B yielded poor nanoparticles, with insufficient covering of silica. Method C, D, and E were much more successful and ensured a reproducible covering of the nanoparticles with a thin but homogeneous layer of silica. The synthesis method that was retained used the following ratio of reagents: ethanol (40 mL), 25% NH_3 (2 mL), and TEOS (0.8 mL) (method E). This method yields nanoparticles with a homogeneous $4.8 \pm 0.5\text{ nm}$ thick SiO_2 shell (TEM). This thickness is the right compromise between a good protection of the nanoparticle core, without losing too much surface area.

The functionalization parameters have great influence on the quality of the functional coating. The functionalization reaction of $\text{Fe}_3\text{O}_4@\text{SiO}_2$ nanoparticles with TMS-EDTA is pH-dependent because the hydrolysis rate of the alkoxy silanes is pH-controlled.³³ Acidic conditions are required for the controlled silanization of the surface (pH 3–5) because an alkaline pH causes rapid polymerization of the silane chains.^{33,34} The solvent composition is also important. Water increases the

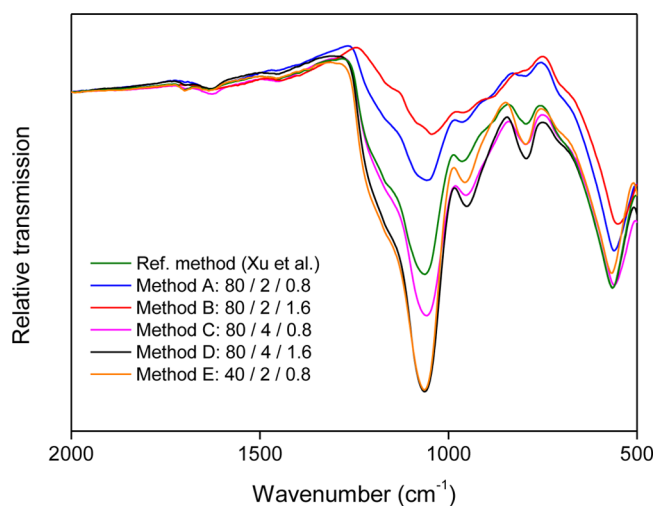


Figure 2. FTIR spectra of $\text{Fe}_3\text{O}_4@\text{SiO}_2$ samples from different synthesis methods. The influence of the reagent ratio on the Si–O peak at 1091 cm^{-1} is shown. The ratio of reagents is given as ethanol (mL)/25% NH_3 (mL)/TEOS (mL).

hydrolysis rate while methanol slows it down. Different methanol/water ratios were tested to optimize the degree of functionalization (Figure 3) The success of the functionaliza-

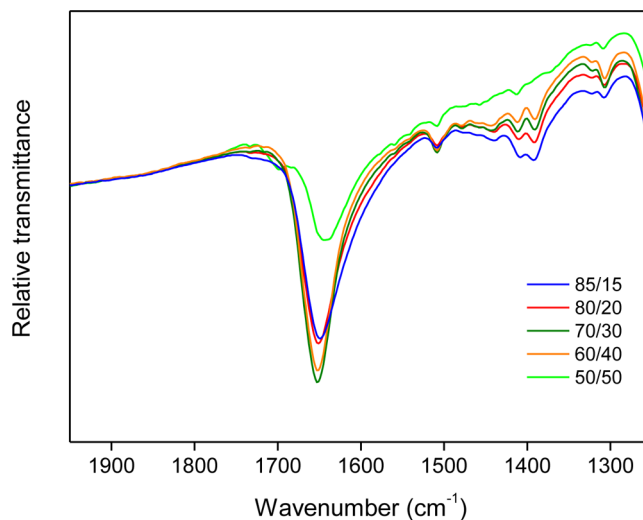


Figure 3. FTIR spectra of different $\text{Fe}_3\text{O}_4@\text{SiO}_2(\text{TMS-EDTA})$ samples. The influence of the solvent (MeOH/ H_2O ratio) on the carboxylate peaks at 1650 and 1400 cm^{-1} is shown. This signal is related to the degree of TMS-EDTA functionalization.

tion was monitored by FTIR spectroscopy by looking at the intensity of the carboxylate bands.⁷ The compiled FTIR spectra (Figure 3) show the intense asymmetrical stretch of the carboxylate groups around 1650 cm^{-1} accompanied by the symmetrical stretch around 1400 cm^{-1} . Pure methanol was not an ideal solvent for the hydrophilic TMS-EDTA and caused partial precipitation, whereas pure water caused a too fast hydrolysis of the silanes resulting in rapid polymerization and a bad functionalization. A methanol/water volume ratio of 85:15 was chosen because of the reproducibility and the high quality of the functional coating prepared under these conditions.

Characterization of Nanoparticles. The core–shell $\text{Fe}_3\text{O}_4@\text{SiO}_2(\text{TMS-EDTA})$ nanoparticles were characterized

by FTIR, CHN, TGA, BET, and TEM analysis. All TGA curves for $\text{Fe}_3\text{O}_4@\text{SiO}_2$ and $\text{Fe}_3\text{O}_4@\text{SiO}_2(\text{TMS-EDTA})$ can be found in the Supporting Information (Figure S2). The average TMS-EDTA content obtained from CHN analysis was 4.2 ± 0.3 wt %, compared to 3.0 wt % determined by TGA analysis. The average of both analytical techniques was used, which indicates that the nanoparticles contain $0.12 \mu\text{mol}/\text{mg}$ TMS-EDTA. This value is useful for comparison with the adsorption experiments. Vibrating sample magnetometry showed that the superparamagnetic $\text{Fe}_3\text{O}_4(\text{NOA})$ seeds had a saturation magnetization of 66 emu/g (Supporting Information, Figure S1). TEM images showed that the functionalized core-shell $\text{Fe}_3\text{O}_4@\text{SiO}_2(\text{TMS-EDTA})$ nanoparticles had a diameter of 24.1 ± 4.0 nm (Figure 4B). The $\text{Fe}_3\text{O}_4(\text{NOA})$ seeds had a relatively well-

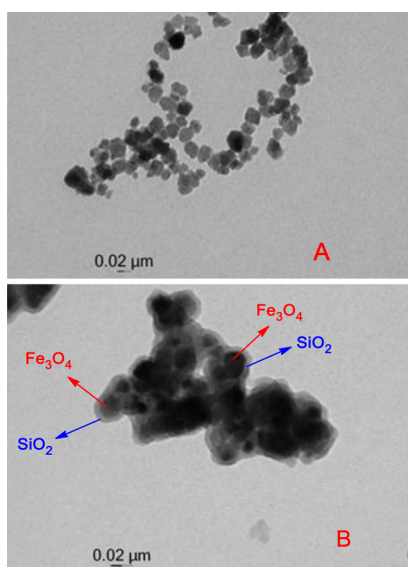


Figure 4. TEM images of (A) $\text{Fe}_3\text{O}_4(\text{NOA})$ seeds and (B) $\text{Fe}_3\text{O}_4@\text{SiO}_2(\text{TMS-EDTA})$ nanoparticles. The magnetic core and the thin homogeneous SiO_2 shell are indicated on image B.

defined spherical shape and an average diameter of 14.5 ± 3.0 nm (Figure 4A). The SiO_2 shell on the core-shell $\text{Fe}_3\text{O}_4@\text{SiO}_2$ nanoparticles had a thickness of 4.8 ± 0.5 nm (Figure 4B). The aggregation of the core-shell nanoparticles in Figure 4 is due to the TEM sample preparation. During the solvent evaporation the nanoparticles aggregate on the grid.

Since the SiO_2 shell is thin and homogeneous, this results in a relatively high specific surface area. The specific surface area of the nanoparticles was $44.1 \text{ m}^2/\text{g}$ as determined by surface analysis using the BET method. This is an important characteristic for a sorbent nanoparticle. A thin SiO_2 shell is also important to maintain a high magnetic susceptibility, required for a fast magnetic removal of the nanoparticles from solution. The core-shell $\text{Fe}_3\text{O}_4@\text{SiO}_2(\text{TMS-EDTA})$ nanoparticles are quite hydrophilic due to the deprotonated carboxylate groups, thus forming very homogeneous and stable dispersions at pH 6 (used for adsorption experiments). Once they bind lanthanide ions, the surface charge diminishes and the nanoparticles can be removed from solution efficiently. Full retrieval (>99.9%) was possible within 10 s (Figure 5). Additionally, during stripping the carboxylate groups are protonated due to the acidic conditions (pH 1.5), making them less hydrophilic and therefore easy to retrieve. This greatly facilitates the adsorption/stripping process.



Figure 5. Magnetic retrieval of $\text{Fe}_3\text{O}_4@\text{SiO}_2(\text{TMS-EDTA})$ nanoparticles dispersed in water (1 mg/mL), before (left) and after 10 s (right).

Adsorption and Stripping of Rare Earths. The adsorption of rare earths is pH-dependent because TMS-EDTA contains three carboxylic acid groups that are gradually deprotonated at increasing pH values. An excess of rare-earth ions was used and the samples were shaken for 18 h to ensure that a maximal adsorption was reached. Nd^{3+} was chosen as a model system because of its industrial relevance. Complex formation was observed between pH 3 and 6 (Figure 6). The

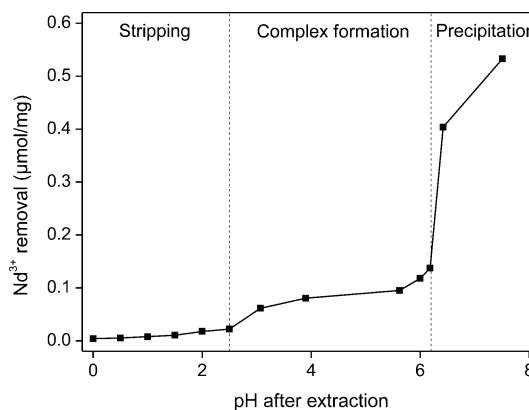


Figure 6. Nd^{3+} removal from solution by $\text{Fe}_3\text{O}_4@\text{SiO}_2(\text{TMS-EDTA})$ nanoparticles as a function of pH. Depending on the pH, different domains were identified where the Nd^{3+} could be adsorbed by the nanoparticles, precipitated, or stripped back from the nanoparticles.

excess of rare-earth ions helps to visualize the precipitation threshold. There is still complex formation at pH values higher than 6, but also hydrolysis and precipitation of the lanthanide ions. This pH range is therefore not convenient since the precipitation interferes with the complex formation. Below pH 2.5, the Nd^{3+} adsorption is quite low; therefore this lower pH range can be used to strip the lanthanide ions from the nanoparticles.

Adsorption of rare-earth ions is best performed at pH 6, resulting in an adsorption of $0.118 \mu\text{mol}/\text{mg}$ (17.0 mg/g) for Nd^{3+} . An excess of Nd^{3+} was used to obtain the maximal adsorption capacity. This value ($0.118 \mu\text{mol}/\text{mg}$) is in good agreement with the TMS-EDTA content on the surface of the nanoparticle ($0.12 \mu\text{mol}/\text{mg}$). If the adsorption capacity is compared with other nanoparticles described in the literature (Table 1), it is well within the range of most reported chelating nanoparticles. However, the main advantage of these nano-

Table 1. Literature Overview of Magnetic Chelating Nanoparticles with Their Maximal Adsorption Capacity, Compared with the Nanoparticles Described in This Work^{8,16,20,21,26,46,47}

particle(ligand)	particle size (nm)	surf. group content (wt %)	ion	ion uptake (mg/g)
Fe ₃ O ₄ @SiO ₂ (TMS-EDTA) ^a	24.1	3.6	Nd ³⁺	17.0
Fe ₃ O ₄ (TMS-EDTA) ²⁶	10.5	Gd ³⁺	113	
Fe ₃ O ₄ (humic acid) ²¹	14	15.5	Eu ³⁺	10.6
Fe ₃ O ₄ @SiO ₂ (P507) ¹⁶	500	13.9	La ³⁺	55.9
Fe ₃ O ₄ (PEI)(DTPA) ²⁰	50	6.4	Cu ²⁺	12.1
Fe ₃ O ₄ (EDTA) ⁸	312.3	7.8	Cu ²⁺	46.3
Fe ₃ O ₄ (chitosan) ⁴⁷	13.5	4.9	Cu ²⁺	21.5
Fe ₃ O ₄ (dien) ⁴⁶	11.6	N/A	Cu ²⁺	12.43

^aThis is the core-shell nanoparticle described in this paper.

particles is not their adsorption capacity, but their selectivity and ability to separate rare-earth ions from each other.

The adsorption kinetics were also investigated by contacting the nanoparticles with an excess of Nd³⁺ ions at pH 6.0 for increasing periods of time (mechanical shaker, 240 rpm). The results show a saturation of the nanoparticles with Nd³⁺ ions after 6 h (Figure 7). However, during most adsorption

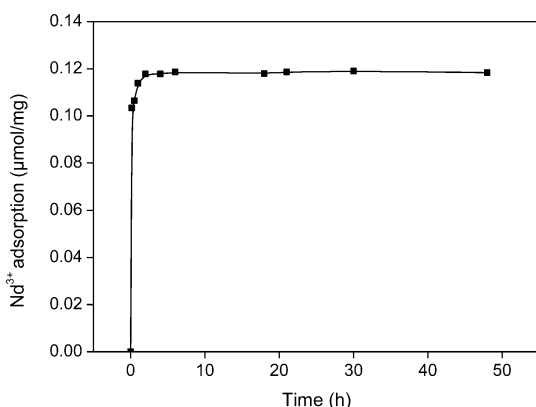


Figure 7. Adsorption kinetics for Nd³⁺ ions with Fe₃O₄@SiO₂(TMS-EDTA) nanoparticles.

experiments the samples were shaken overnight (18 h) for convenience. The relatively long equilibrium times are attributed to the dense layer of EDTA on the surface, which is also responsible for the better than expected size-based selectivity that was observed (see Separation of Rare Earths).

The stripping efficiency as a function of pH was tested, together with the stability of the core-shell nanoparticles. After the nanoparticles were fully loaded with a solution containing an excess of Nd³⁺ ions, the nanoparticles were isolated. The nanoparticles were then contacted with an acidic solution to protonate the carboxylate groups and release the Nd³⁺ ions back in solution. For this stripping step, the pH was set using HCl (1 M) and the solutions were shaken for 2 h (same result as for 24 h). The damage to the nanoparticles was measured by analyzing the iron content in the stripping solution with TXRF, after 24 h of shaking. This iron content was then translated into a particle loss (percent). Stripping is best performed at pH 1.5 in order to have the right compromise between a high stripping efficiency (94%) and little damage to the nanoparticles (<0.5% particle loss) (Figure 8).

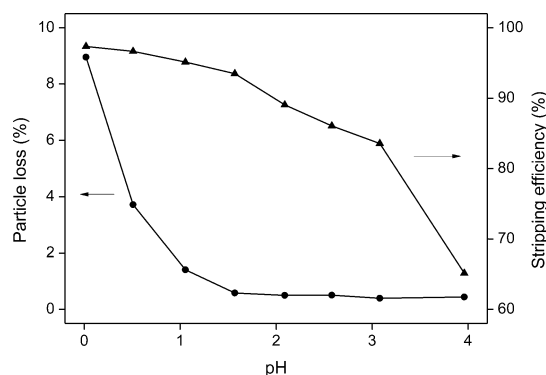


Figure 8. Stripping efficiency and particle loss (determined by TXRF) as a function of pH for core-shell nanoparticles, fully loaded with Nd³⁺ ions.

By comparing the stability of the core-shell nanoparticles with the simple (core) magnetite nanoparticles, it is clear that the SiO₂ shell significantly increased the resistance of magnetite nanoparticles to acidic solutions (Figure 9). The SiO₂ shell is

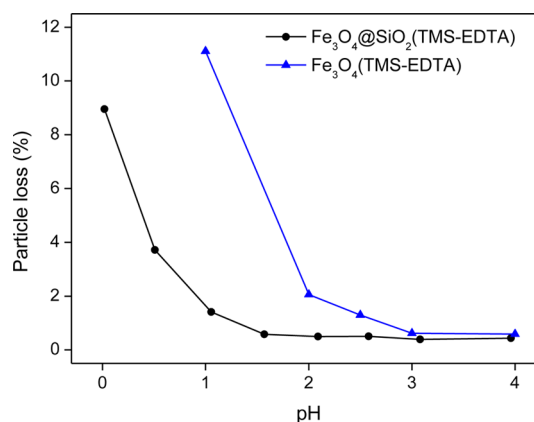


Figure 9. Stability of functionalized magnetite nanoparticles compared with the stability of functionalized core-shell nanoparticles after shaking for 24 h in an acidic solution. The pH was set with an HCl solution.

only 4.8 nm thick, but it drastically increases the stability of the nanoparticles. SiO₂ is much less sensitive to degradation by HCl than Fe₃O₄ that is easily dissolved as FeCl₃. The increased stability of core-shell nanoparticles in acidic solutions is particularly useful for metal binding surface groups that require harsher stripping conditions.

This increased stability is also translated into a good reusability. A sequence of five adsorption (pH 6.0) and stripping (pH 1.5) cycles with an excess of Nd³⁺ ions shows the evolution of the adsorption capacity of the core-shell nanoparticles (Figure 10). The experiments were done three times to reduce the experimental error. During the first cycle, a loss of adsorption capacity was observed from 0.118 to 0.092 μmol/mg. This is due to the release of some of the less well bonded TMS-EDTA groups or some irreversible adsorption. During the functionalization, some of the TMS-EDTA groups are weakly bound to other TMS-EDTA groups through one Si-O-Si linker. This partial oligomerization is an unavoidable phenomenon for trialkoxysilanes; however, most TMS-EDTA groups are firmly attached to the SiO₂ surface with three Si-O-Si bonds.³⁶ After this initial drop in adsorption capacity, the

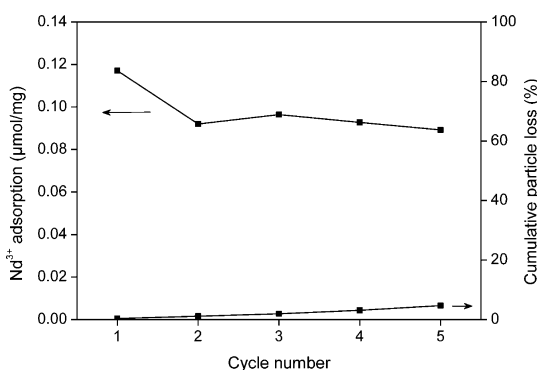


Figure 10. Evolution of adsorption capacity and particle loss over five adsorption/stripping cycles of Nd³⁺ ions with Fe₃O₄@SiO₂(TMS-EDTA) nanoparticles.

adsorption capacity then stabilized and remained practically unchanged over the next four adsorption/stripping cycles. The initial drop in adsorption capacity can be avoided by washing the synthesized nanoparticles one time with a pH 1.5 HCl solution, before using them in adsorption experiments. The particle loss in each cycle increased slightly from 0.3% in cycle 1 to 1.6% in cycle 5, resulting in a cumulated particle loss of 4.7%. Furthermore, it should be mentioned that no particle degradation was observed visually. The supernatant remained completely colorless (Figure 5). This indicates that the particle loss is very limited and is most likely also due to process steps. The particles have to be transferred multiple times in different flasks, inevitably leading to some loss of particles along the way. Small quantities of nanoparticles were used (10 mg); therefore the percent particle loss seems higher even though only 0.47 mg of particles was lost after five adsorption/stripping cycles. The average stripping efficiency over the five cycles was 93%, which is in agreement with previously mentioned results (Figure 8).

Separation of Rare Earths. The separation of rare earths as a group from other elements is usually relatively efficient, and based on differences in oxidation state or chemical behavior.⁴⁸ However, the mutual separation of a mixture of rare-earth ions is a challenge because of their common +III oxidation state and very similar chemical behavior. Most current techniques are based on the small differences in ionic radii.⁴² The selectivity of the functionalized core-shell nanoparticles was investigated and reported using enrichment factors (EFs). The enrichment factor compares the molar ratio of elements A and B before and after separation, according to eq 1. B was chosen to be the heavier (smaller) of the two rare-earth ions because this results in an enrichment factor of >1.

$$EF = \frac{\left(\frac{B}{A}\right)_{\text{on nanoparticles}}}{\left(\frac{B}{A}\right)_{\text{feed solution}}} \quad (1)$$

The separation of Er³⁺/La³⁺ was chosen as a model to investigate the influence of the pH on the selectivity. The relatively large difference in ionic radius results in a high enrichment factor which helps to visualize a possible trend. An excess of rare-earth ions was used compared to the amount of TMS-EDTA groups and the rare-earth pairs were present in a 1:1 molar ratio. The core-shell Fe₃O₄@SiO₂(TMS-EDTA) nanoparticles display the highest selectivity around pH 6 (Figure 11). At this pH, TMS-EDTA also has a high adsorption

capacity and selectivity. Higher pH values cause hydrolysis and precipitation of lanthanide ions (Figure 6).

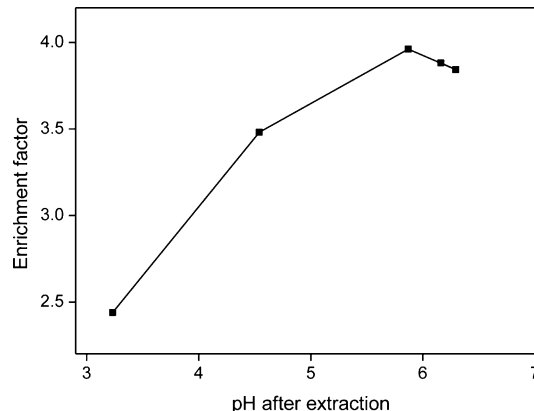


Figure 11. Influence of pH on separation of Er³⁺/La³⁺ by core-shell Fe₃O₄@SiO₂(TMS-EDTA) nanoparticles.

Furthermore, the selectivity of the core-shell Fe₃O₄@SiO₂(TMS-EDTA) nanoparticles toward different pairs of lanthanide ions was investigated and compared with previously published results for Fe₃O₄(TMS-EDTA) and SiO₂(TMS-EDTA).²⁶ Ln³⁺/La³⁺ separations showed that the core-shell nanoparticles behaved similarly to SiO₂(TMS-EDTA) (Figure 12).

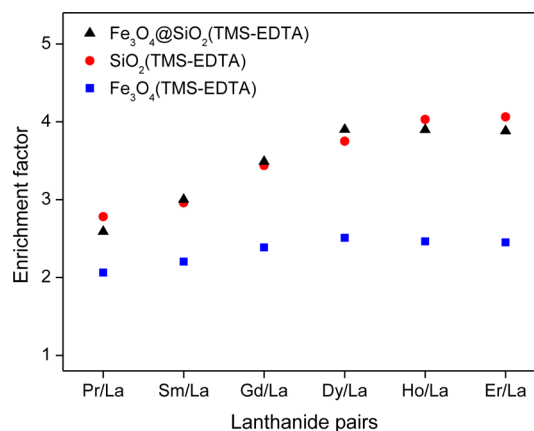


Figure 12. Separation of Ln³⁺/La³⁺ rare-earth pairs (pH 6.0) with increasingly different ionic radii from left to right. The results for Fe₃O₄@SiO₂(TMS-EDTA) particles are compared with previously published data for Fe₃O₄(TMS-EDTA) and SiO₂(TMS-EDTA) nanoparticles.²⁶

One can notice that the enhanced selectivity of TMS-EDTA on SiO₂ substrates was also observed for the core-shell nanoparticles.²⁶ This further supports the hypothesis that the higher density of TMS-EDTA groups on SiO₂ surfaces is responsible for this enhanced size-based selectivity.²⁶ It must be noted that the enrichment factor increases rapidly at the beginning of the Ln³⁺/La³⁺ separation series and stagnates for the heaviest lanthanides. This is a well-known trend for solvent extraction and aminocarboxylate ligands.^{42,43} Another explanation for this can be that the heavier (smaller) lanthanide ions are able to penetrate the dense TMS-EDTA surface layer more easily, making the size-based selectivity less efficient.

4. CONCLUSIONS

Core-shell $\text{Fe}_3\text{O}_4@\text{SiO}_2$ nanoparticles were synthesized and functionalized with metal-coordinating TMS-EDTA groups. The idea was that this type of hybrid nanoparticles could combine the advantage of magnetic retrieval (Fe_3O_4 core) with the higher selectivity that had been observed when TMS-EDTA was attached to SiO_2 compared to Fe_3O_4 nanoparticles.²⁶ Thin and homogeneous SiO_2 shells (4.8 ± 0.5 nm thick) were grown around Fe_3O_4 cores (14.5 ± 3.0 nm diameter), using a modified and optimized Stöber method. This synthesis protocol allowed synthesizing high-quality $\text{Fe}_3\text{O}_4@\text{SiO}_2(\text{TMS-EDTA})$ nanoparticles. It was also shown that the functionalized SiO_2 shell offers a good size-based separation of rare-earth ions similar to the selectivity that had been previously observed for $\text{SiO}_2(\text{TMS-EDTA})$ nanoparticles, but with the added advantage of magnetic retrieval.²⁶ The fact that these core-shell nanoparticles combine the advantages of both the possibility of magnetic retrieval and a high selectivity for metal sorption makes this a very interesting sorbent for the selective recovery of rare-earth ions from dilute aqueous solutions. The nanoparticles showed a good chemical stability even in strongly acidic environments thanks to the SiO_2 shell. The reusability of the nanoparticles was also satisfactory with the adsorption capacity remaining stable after the first adsorption/stripping cycle.

■ ASSOCIATED CONTENT

📄 Supporting Information

VSM measurement of the magnetite seed particles $\text{Fe}_3\text{O}_4(\text{NOA})$ and TGA measurements for $\text{Fe}_3\text{O}_4@\text{SiO}_2$ and $\text{Fe}_3\text{O}_4@\text{SiO}_2(\text{TMS-EDTA})$. Infrared spectra of Fe_3O_4 , $\text{Fe}_3\text{O}_4@\text{SiO}_2$, and $\text{Fe}_3\text{O}_4@\text{SiO}_2(\text{TMS-EDTA})$ nanoparticles. This material is available free of charge via the Internet at <http://pubs.acs.org>.

■ AUTHOR INFORMATION

Corresponding Author

*E-mail: Koen.Binnemans@chem.kuleuven.be.

Notes

The authors declare no competing financial interest.

■ ACKNOWLEDGMENTS

The authors thank the KU Leuven (Projects GOA/13/008 and IOF-KP RARE³) and the FWO Flanders (Ph.D. fellowship to D.D.) for financial support. CHN analyses were performed by Dirk Henot, and TGA measurements were performed by Danny Winant and Dr. Stijn Schaltin. VSM was measured by Ward Brullot, and the BET surface analysis was performed by Ivo Stassen.

■ REFERENCES

- (1) Hao, R.; Xing, R.; Xu, Z.; Hou, Y.; Gao, S.; Sun, S. Synthesis, Functionalization, and Biomedical Applications of Multifunctional Magnetic Nanoparticles. *Adv. Mater.* **2010**, *22*, 2729.
- (2) Lu, A.-H.; Salabas, E. L.; Schüth, F. Magnetic Nanoparticles: Synthesis, Protection, Functionalization, and Application. *Angew. Chem., Int. Ed.* **2007**, *46*, 1222.
- (3) Grass, R. N.; Athanassiou, E. K.; Stark, W. J. Covalently Functionalized Cobalt Nanoparticles as a Platform for Magnetic Separations in Organic Synthesis. *Angew. Chem., Int. Ed.* **2007**, *46*, 4909.
- (4) Liu, Z.; Li, B.; Wang, B.; Yang, Z.; Wang, Q.; Li, T.; Qin, D.; Li, Y.; Wang, M.; Yan, M. Magnetic Nanoparticles Modified with DTPA-

AMC-Rare Earth for Fluorescent and Magnetic Resonance Dual Mode Imaging. *Dalton Trans.* **2012**, *41*, 8723.

- (5) Wang, B.; Hai, J.; Wang, Q.; Li, T.; Yang, Z. Coupling of Luminescent Terbium Complexes to Fe_3O_4 Nanoparticles for Imaging Applications. *Angew. Chem., Int. Ed.* **2011**, *50*, 3063.

- (6) Xi, P.; Cheng, K.; Sun, X.; Zeng, Z.; Sun, S. Magnetic Fe_3O_4 Nanoparticles Coupled with a Fluorescent Eu Complex for Dual Imaging Applications. *Chem. Commun.* **2012**, *48*, 2952.

- (7) Goon, I. Y.; Zhang, C.; Lim, M.; Gooding, J. J.; Amal, R. Controlled Fabrication of Polyethylenimine-Functionalized Magnetic Nanoparticles for the Sequestration and Quantification of Free Cu^{2+} . *Langmuir* **2010**, *26*, 12247.

- (8) Liu, Y.; Chen, M.; Yongmei, H. Study on the Adsorption of Cu(II) by EDTA Functionalized Fe_3O_4 Magnetic Nano-Particles. *Chem. Eng. J.* **2013**, *218*, 46.

- (9) Ren, Y.; Abbood, H. A.; He, F.; Peng, H.; Huang, K. Magnetic EDTA-modified Chitosan/ $\text{SiO}_2/\text{Fe}_3\text{O}_4$ Adsorbent: Preparation, Characterization, and Application in Heavy Metal Adsorption. *Chem. Eng. J.* **2013**, *226*, 300.

- (10) Sun, L.; Li, Y.; Sun, M.; Wang, H.; Xu, S.; Zhang, C.; Yang, Q. Porphyrin-Functionalized $\text{Fe}_3\text{O}_4@\text{SiO}_2$ Core/Shell Magnetic Colorimetric Material for Detection, Adsorption and Removal of Hg^{2+} in Aqueous Solution. *New J. Chem.* **2011**, *35*, 2697.

- (11) Warner, C. L.; Addleman, R. S.; Cinson, A. D.; Droubay, T. C.; Engelhard, M. H.; Nash, M. A.; Yantasee, W.; Warner, M. G. High-Performance, Superparamagnetic, Nanoparticle-Based Heavy Metal Sorbents for Removal of Contaminants from Natural Waters. *ChemSusChem* **2010**, *3*, 749.

- (12) Rossier, M.; Koehler, F. M.; Athanassiou, E. K.; Grass, R. N.; Aeschlimann, B.; Gunther, D.; Stark, W. J. Gold Adsorption on the Carbon Surface of C/Co Nanoparticles Allows Magnetic Extraction from Extremely Diluted Aqueous Solutions. *J. Mater. Chem.* **2009**, *19*, 8239.

- (13) Rossier, M.; Koehler, F. M.; Athanassiou, E. K.; Grass, R. N.; Waelle, M.; Birbaum, K.; Günther, D.; Stark, W. J. Energy-Efficient Noble Metal Recovery by the Use of Acid-stable Nanomagnets. *Ind. Eng. Chem. Res.* **2010**, *49*, 9355.

- (14) Yantasee, W.; Warner, C. L.; Sangvanich, T.; Addleman, R. S.; Carter, T. G.; Wiacek, R. J.; Fryxell, G. E.; Timchalk, C.; Warner, M. G. Removal of Heavy Metals from Aqueous Systems with Thiol Functionalized Superparamagnetic Nanoparticles. *Environ. Sci. Technol.* **2007**, *41*, 5114.

- (15) Hao, Y.-M.; Man, C.; Hu, Z.-B. Effective Removal of Cu (II) Ions from Aqueous Solution by Amino-functionalized Magnetic Nanoparticles. *J. Hazard. Mater.* **2010**, *184*, 392.

- (16) Wu, D.; Sun, Y.; Wang, Q. Adsorption of Lanthanum (III) from Aqueous Solution Using 2-ethylhexyl Phosphonic Acid Mono-2-ethylhexyl Ester-Grafted Magnetic Silica Nanocomposites. *J. Hazard. Mater.* **2013**, *260*, 409.

- (17) Saiz, J.; Bringas, E.; Ortiz, I. New Functionalized Magnetic Materials for As^{5+} Removal: Adsorbent Regeneration and Reuse. *Ind. Eng. Chem. Res.* **2014**, DOI: 10.1021/ie500912k.

- (18) Zargoosh, K.; Abedini, H.; Abdolmaleki, A.; Molavian, M. R. Effective Removal of Heavy Metal Ions from Industrial Wastes Using Thiosalicylhydrazide-Modified Magnetic Nanoparticles. *Ind. Eng. Chem. Res.* **2013**, *52*, 14944.

- (19) Zhang, F.; Shi, Y.; Zhao, Z.; Ma, B.; Wei, L.; Lu, L. Amino-functionalized $\text{Fe}_3\text{O}_4/\text{SiO}_2$ Magnetic Submicron Composites and In^{3+} Ion Adsorption Properties. *J. Mater. Sci.* **2014**, *49*, 3478.

- (20) Koehler, F. M.; Rossier, M.; Waelle, M.; Athanassiou, E. K.; Limbach, L. K.; Grass, R. N.; Gunther, D.; Stark, W. J. Magnetic EDTA: coupling heavy metal chelators to metal nanomagnets for rapid removal of cadmium, lead and copper from contaminated water. *Chem. Commun.* **2009**, 4862.

- (21) Yang, S.; Zong, P.; Ren, X.; Wang, Q.; Wang, X. Rapid and Highly Efficient Preconcentration of Eu(III) by Core-Shell Structured $\text{Fe}_3\text{O}_4@\text{Humic Acid}$ Magnetic Nanoparticles. *ACS Appl. Mater. Interfaces* **2012**, *4*, 6891.

- (22) Xu, Y.; Zhou, Y.; Ma, W.; Wang, S.; Li, S. Functionalized Magnetic Core-shell $\text{Fe}_3\text{O}_4@/\text{SiO}_2$ Nanoparticles for Sensitive Detection and Removal of Hg^{2+} . *J. Nanopart. Res.* **2013**, *15*, 1.
- (23) Li, Y.; Wu, J.; Qi, D.; Xu, X.; Deng, C.; Yang, P.; Zhang, X. Novel Approach for the Synthesis of $\text{Fe}_3\text{O}_4@/\text{TiO}_2$ Core-Shell Microspheres and their Application to the Highly Specific Capture of Phosphopeptides for MALDI-TOF MS Analysis. *Chem. Commun.* **2008**, *5*, 564.
- (24) Huang, C.; Hu, B. Silica-coated Magnetic Nanoparticles Modified with γ -Mercaptopropyltrimethoxysilane for Fast and Selective Solid Phase Extraction of Trace Amounts of Cd, Cu, Hg, and Pb in Environmental and Biological Samples Prior to their Determination by Inductively Coupled Plasma Mass Spectrometry. *Spectrochim. Acta, Part B* **2008**, *63*, 437.
- (25) Saman, N.; Johari, K.; Mat, H. Adsorption Characteristics of Sulfur-Functionalized Silica Microspheres with Respect to the Removal of $\text{Hg}(\text{II})$ from Aqueous Solutions. *Ind. Eng. Chem. Res.* **2014**, *53*, 1225.
- (26) Dupont, D.; Brullot, W.; Bloemen, M.; Verbiest, T.; Binnemans, K. Selective Uptake of Rare Earths from Aqueous Solutions by EDTA-functionalized Magnetic and Non-magnetic Nanoparticles. *ACS Appl. Mater. Interfaces* **2014**, *6*, 4980.
- (27) Wei, S.; Wang, Q.; Zhu, J.; Sun, L.; Lin, H.; Guo, Z. Multifunctional Composite Core-Shell Nanoparticles. *Nanoscale* **2011**, *3*, 4474.
- (28) Scharl, W. Current Directions in Core-shell Nanoparticle Design. *Nanoscale* **2010**, *2*, 829.
- (29) Ghosh Chaudhuri, R.; Paria, S. Core/Shell Nanoparticles: Classes, Properties, Synthesis Mechanisms, Characterization, and Applications. *Chem. Rev.* **2011**, *112*, 2373.
- (30) Morel, A.-L.; Nikitenko, S. I.; Gionnet, K.; Wattiaux, A.; Lai-Kee-Him, J.; Labrugere, C.; Chevalier, B.; Deleris, G.; Petibois, C.; Brisson, A.; Simonoff, M. Sonochemical Approach to the Synthesis of $\text{Fe}_3\text{O}_4@/\text{SiO}_2$ Core-Shell Nanoparticles with Tunable Properties. *ACS Nano* **2008**, *2*, 847.
- (31) Hui, C.; Shen, C.; Tian, J.; Bao, L.; Ding, H.; Li, C.; Tian, Y.; Shi, X.; Gao, H.-J. Core-shell $\text{Fe}_3\text{O}_4@/\text{SiO}_2$ Nanoparticles Synthesized with Well-dispersed Hydrophilic Fe_3O_4 Seeds. *Nanoscale* **2011**, *3*, 701.
- (32) Ding, H. L.; Zhang, Y. X.; Wang, S.; Xu, J. M.; Xu, S. C.; Li, G. H. $\text{Fe}_3\text{O}_4@/\text{SiO}_2$ Core/Shell Nanoparticles: The Silica Coating Regulations with a Single Core for Different Core Sizes and Shell Thicknesses. *Chem. Mater.* **2012**, *24*, 4572.
- (33) Witucki, G. L. A Silane Primer—Chemistry and Applications of Alkoxy Silanes. *J. Coat. Technol.* **1993**, *65*, 57.
- (34) Hermanson, G. T. In *Bioconjugate Techniques*, 2nd ed.; Hermanson, G. T., Ed.; Academic Press: New York, 2008; pp 562–581.
- (35) De Palma, R.; Peeters, S.; Van Bael, M. J.; Van den Rul, H.; Bonroy, K.; Laureyn, W.; Mullens, J.; Borghs, G.; Maes, G. Silane Ligand Exchange to Make Hydrophobic Superparamagnetic Nanoparticles Water-Dispersible. *Chem. Mater.* **2007**, *19*, 1821.
- (36) Fadeev, A. Y.; McCarthy, T. J. Self-Assembly Is Not the Only Reaction Possible Between Alkyltrichlorosilanes and Surfaces: Monomolecular and Oligomeric Covalently Attached Layers of Dichloro- and Trichloroalkylsilanes on Silicon. *Langmuir* **2000**, *16*, 7268.
- (37) Onclin, S.; Ravoo, B. J.; Reinhoudt, D. N. Engineering Silicon Oxide Surfaces Using Self-Assembled Monolayers. *Angew. Chem., Int. Ed.* **2005**, *44*, 6282.
- (38) Tucker-Schwartz, A. K.; Farrell, R. A.; Garrell, R. L. Thiol-ene Click Reaction as a General Route to Functional Trialkoxysilanes for Surface Coating Applications. *J. Am. Chem. Soc.* **2011**, *133*, 11026.
- (39) Larsen, B. A.; Hurst, K. M.; Ashurst, W. R.; Serkova, N. J.; Stoldt, C. R. Mono and Dialkoxysilane Surface Modification of Superparamagnetic Iron Oxide Nanoparticles for Application as Magnetic Resonance Imaging Contrast Agents. *J. Mater. Res.* **2012**, *27*, 1846.
- (40) Bloemen, M.; Brullot, W.; Luong, T. T.; Geukens, N.; Gils, A.; Verbiest, T. Improved Functionalization of Oleic Acid-Coated Iron Oxide Nanoparticles for Biomedical Applications. *J. Nanopart. Res.* **2012**, *14*, 1100.
- (41) Wu, W.; He, Q. G.; Jiang, C. Z. Magnetic Iron Oxide Nanoparticles: Synthesis and Surface Functionalization Strategies. *Nanoscale Res. Lett.* **2008**, *3*, 397.
- (42) Xie, F.; Zhang, T. A.; Dreisinger, D.; Doyle, F. A Critical Review on Solvent Extraction of Rare Earths from Aqueous Solutions. *Miner. Eng.* **2014**, *56*, 10.
- (43) Choppin, G. R.; Goedken, M. P.; Gritmon, T. F. The Complexation of Lanthanides by Aminocarboxylate Ligands—II. *J. Inorg. Nucl. Chem.* **1977**, *39*, 2025.
- (44) Cotton, S. In *Lanthanide and Actinide Chemistry*; Wiley: Chichester, U.K., 2006; Chapter 4, pp 35–60.
- (45) Brullot, W.; Reddy, N. K.; Wouters, J.; Valev, V. K.; Goderis, B.; Vermant, J.; Verbiest, T. Versatile Ferrofluids Based on Polyethylene Glycol Coated Iron Oxide Nanoparticles. *J. Magn. Magn. Mater.* **2012**, *324*, 1919.
- (46) Huang, S.-H.; Chen, D.-H. Rapid Removal of Heavy Metal Cations and Anions from Aqueous Solutions by an Amino-functionalized Magnetic Nano-Adsorbent. *J. Hazard. Mater.* **2009**, *163*, 174.
- (47) Chang, Y.-C.; Chen, D.-H. Preparation and Adsorption Properties of Monodisperse Chitosan-Bound Fe_3O_4 Magnetic Nanoparticles for Removal of $\text{Cu}(\text{II})$ Ions. *J. Colloid Interface Sci.* **2005**, *283*, 446.
- (48) Vander Hoogerstraete, T.; Wellens, S.; Verachtert, K.; Binnemans, K. Removal of Transition Metals from Rare earths by Solvent Extraction with an Undiluted Phosphonium Ionic Liquid: Separations Relevant to Rare-earth Magnet Recycling. *Green Chem.* **2013**, *15*, 919.